Motion-control analysis of ICPF-actuated underwater biomimetic microrobots

Baofeng Gao*

Graduate School of Engineering,
Kagawa University,
2217-20, Hayashi-cho, Takamatsu, 761-0396, Japan
E-mail: s08d504@stmail.eng.kagawa-u.ac.jp
*Corresponding author

Shuxiang Guo

Faculty of Engineering,
Kagawa University,
2217-20, Hayashi-cho, Takamatsu, 761-0396, Japan
and
Harbin Engineering University,
145 Nantong Street, Harbin, Heilongjiang 150001, China
E-mail: guo@eng.kagawa-u.ac.jp

Xiufen Ye

Harbin Engineering University,
145 Nantong Street, Harbin, Heilongjiang 150001, China
E-mail: yexiufen@hrbeu.edu.cn

Abstract: This paper introduces the development of biomimetic underwater microrobots consisting of AVR microcontroller, an infrared ray communication system, and ionic conducting polymer film (ICPF) actuators. We use AVR ATmega16 as the control unit and an infrared ray receiver to provide feedback to the AVR unit. The spiral particle pathway searching approach is developed to search for particles. We also use MATLAB and OpenGL to simulate the path planning and optimisation according to the particle swarm optimisation algorithm. We implemented and demonstrated wireless control over the trajectory of individual microrobot, and extended this to three units in an expect formation.

Keywords: underwater biomimetic microrobot; AVR; ionic conducting polymer films (ICPF) actuator; particle swarm optimisation; path planning; optimisation.

Reference to this paper should be made as follows: Gao, B., Guo, S. and Ye, X. (2011) 'Motion-control analysis of ICPF-actuated underwater biomimetic microrobots', *Int. J. Mechatronics and Automation*, Vol. 1, No. 2, pp.79–89.

Biographical notes: Baofeng Gao is currently a PhD student in the Biomechatronics Group at the Kagawa University. He received his Bachelor's degree in College of Mechanical and Electrical Engineering from the Northeast Forestry University, China in 2003 and received his MS degree in Harbin Engineering University, China in 2007. His current research interests include smart material based on actuators, micro robotics and automation, path-planning and optimisation of micro robotics system. He is an IEEE student member and has published several journals and conference papers.

Shuxiang Guo received his PhD in Mechano-Informatics and Systems from the Nagoya University, Nagoya, Japan in 1995. Currently, he is a Professor with the Department of Intelligent Mechanical System Engineering at the Kagawa University. His current research interests include micro robotics and mechatronics, micro robotics system for minimal invasive surgery, micro catheter system, micro pump, and smart material (SMA, ICPF). He received research awards from the Tokai Section of the Japan Society of Mechanical Engineers (JSME), Best Conference Paper Award of the IEEE ROBIO2004 and Best Conference Paper Award of the IEEE ICAL 2008 in 1997, 2004 and 2008, respectively.

Xiufen Ye received her PhD in Control Theory and Control Engineering in 2003 from the Harbin Engineering University, China. Currently, she is a Professor with the Lab. of Biomimetic Microrobot and System, College of Automation, Harbin Engineering University. She has published over 100 journals and conference papers. Her current research interests include networked systems and teleoperation, haptics, pattern recognition and intelligent system, and biomimetic microrobot system. She has served on the organising committees of many conferences.

1 Introduction

With the development of micro techniques and smart materials, coupled with the increasing demands from industry in the field of ocean exploration, a centimetre-scale microrobot system with novel materials, such as ionic conducting polymer films (ICPF), have many potential applications. The invention of underwater microrobot is expected to lead to their increasingly widespread use in industrial, medical, and military applications. For example, maritime countries are investigating new techniques of developing novel materials such as ICPF, and these materials are being investigated as possible materials for artificial muscles and micro-electromechanical systems (MEMS) actuators to drive microrobots (Sadeghipour et al., 1992; Shahinpoor et al., 1998; Ye et al., 2006; Waldner, 2008; Pan et al., 2008; Guo, et al., 2010).

ICPF technology is one of the most exciting research areas in Biological micro-electromechanical system (bio-MEMS) and is paving the way to a great variety of biomimetic approaches for underwater microrobot design. The low actuating voltage and quick bending responses of ICPF are attractive for the construction of various types of actuators and sensors (Guo and Asaka, 2003; Guo and Wang, 2003a; Wei et al., 2010; Guo et al., 2006; Shi et al., 2010; Wei and Guo, 2010; Ye et al., 2010).

The development of the microrobot in our researches can be broken up into three sub-topics, summarised as follows.

1.1 Characteristic analysis and application of ICPF actuators in underwater microrobot systems

ICPF actuators are low-power devices and so are suitable for microrobot applications because of the favourable battery power requirements. The underwater microrobot should be designed to facilitate various motions, including walking and swimming motions, and the ability to control depth below the surface of the water.

The ICPF actuator can drive the microrobot to move forward or turn around, and the speed of the microrobot can be controlled by varying the voltage of the input signal when the frequency of the input signal is fixed at 1 Hz. The ICPF can produce vapour bubbles when the frequency of input voltage signal is lower than 0.3 Hz. According to the characteristics of ICPF, we can input a low-frequency voltage signal to make the material produce vapour bubbles and make the microrobot float upward slowly.

1.2 Development of a novel wireless-controlled ICPF-actuated fish-like underwater microrobot system

We propose a new kind of underwater microrobot system consisting of a mother submarine and several ICPF-actuated microrobots. The mother submarine needs to have enough space to carry microrobots; either remote-operated vehicles (ROVs) or autonomous underwater vehicles (AUVs) could be used as the submarine. When they receive control signals, microrobots can be released from the body of the mother submarine.

The microrobot should have communication unit and be able to share information with each other, and exploiting some multi-robot control method, should cooperate to accomplish a given task (Okuzaki and Osada, 1994; Rus et al., 1995; Jennings et al., 1997; Stone and Veloso, 1999).

The ICPF-actuated underwater microrobot should be controlled wirelessly, and in our system, the underwater microrobots employ Atmel AVR minimum microcontrollers, Infrared Ray Data Association (IRDA) infrared communication systems, and ICPF actuators. ATmega16 was used for the control unit of the microrobot, and the IRDA communications system operated at 940 nm and was used to receive and sent the feedback signal to the AVR unit. A square-wave control signal sent out from the AVR to the electric relay G6S-2 was used to adjust the voltage at the ICPF actuator to control the motion of the microrobot.

Control of the trajectory of individual microrobot was demonstrated experimentally, illustrating the effectiveness of the wireless-control method.

1.3 Motion control and swarm optimisation of the underwater microrobot system

To develop the global path-planning method for the robot system, it was necessary to set up an environmental model that includes information such as the position of microrobot and the shape of obstacles. We also used search algorithms to determine the path-planning fit for the needs of people. Several fundamental modelling methods have been proposed, such as the framework space approach (including the visibility graph, the Voronoi graph, and the tangent graph) (Du et al., 2006), the free-space method, and the grid method.

We used MATLAB to simulate path planning and optimisation according to the particle-swarm-optimisation

(PSO) algorithm when the microrobot meets obstacles. Obstacles were simplified and treated as solid sphere, and the robot can be considered as a point particle. The three-dimensional underwater space was separated into several parts. Drawing upon the concept of the grid method (Lelli et al., 2007), a spiral particle pathway searching approach was developed to search for particles in the pathway in a given plane.

2 Development of the multi-microrobot system

Recently, many kinds of biomimetic underwater microrobots using ICPF actuators have been developed for various purposes, swim and walk underwater (Fukuda et al., 1994; Fukuda et al., 1995; Zhang et al., 2006). ICPF is also used for bipedal underwater robots and multi-DOF (depth of field) manipulators (Kamamichi et al., 2003).

As shown in Figure 3, for the microrobot, when the applied voltage was in the range 2 to 10 V, the tail fin of the microrobot could swing; when the tail fin swings up, it clamps the fluke, producing s backward cascade, and the consequent retroaction force pushes the microrobot forward. Such fish-like biomimetic robots were shown to perform better with both caudal and ventral fins. The microrobot was also capable of walking motion, as shown in Figure 4. However, these microrobots were controlled using wires to transmit signals, and for practical applications, it is far preferable to control microrobots wirelessly (Mojarrad and Shahinpoor, 1997; Klaassen et al., 2002; Nguyen et al., 2009; Zhao and Guo, 2010).

We set up the experiment platform and did the characteristic analysis of ICPF, as shown in Figure 2.

The dynamic mechanism of pushing forward is expressed in equation (1) (Shahinpoor, 1996; Ye et al., 2006):

$$F_d = -\frac{1}{2} C_d \rho A V_k \left| V_k \right| \tag{1}$$

where C_d is the drag coefficient based on wet surface area A, ρ is the density of water, and V_k is the relative velocity between the microrobot and the surface of the water.

Figure 1 ICPF (see online version for colours)

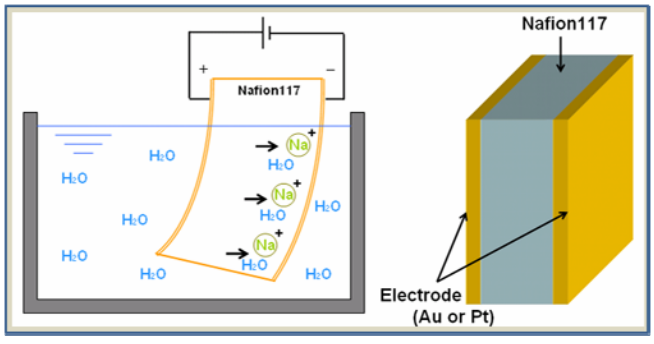

Figure 2 Characteristic analyses of the ICPF actuator (see online version for colours)

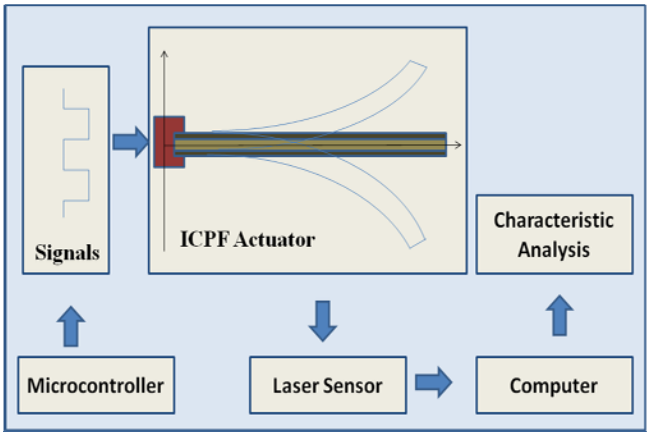

Figure 3 Hybrid type of underwater micro biped robot with walking and swimming motions by Guo Lab., Kagawa University, Japan, 2006 (see online version for colours)

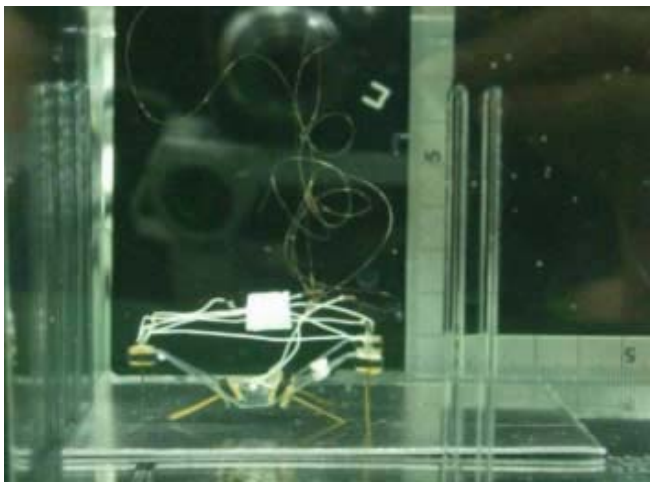

Source: Zhang et al. (2006a)

Figure 4 The ICPF actuator used in the underwater microrobot to generate a walking motion by Guo Lab., Kagawa University, Japan, 2005 (see online version for colours)

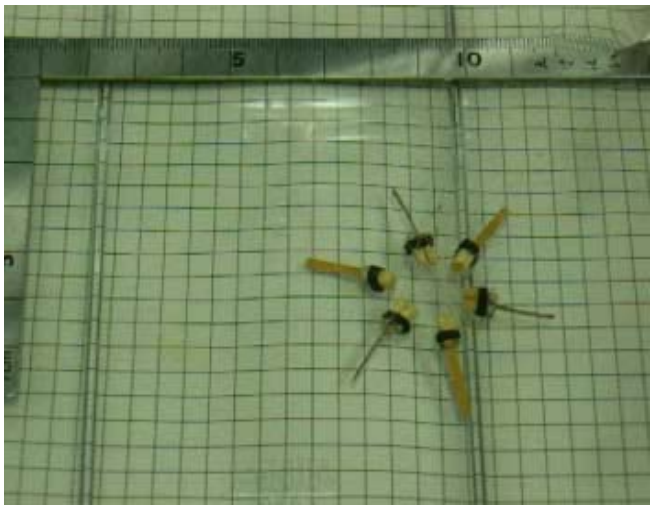

Source: Zhang et al. (2006)

Figure 5 The underwater multi-microrobot system (see online version for colours)

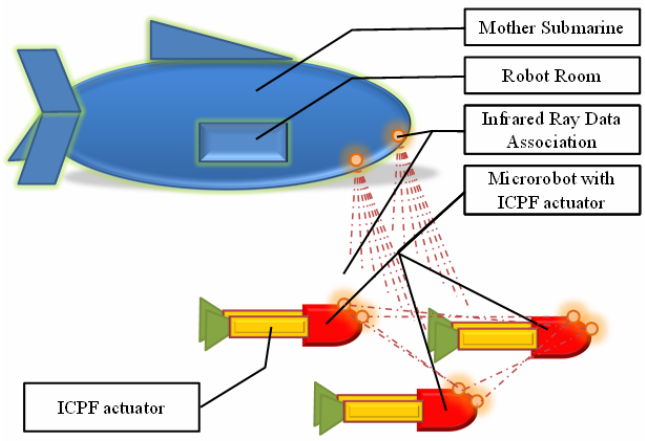

It is difficult for these underwater microrobots to be controlled in certain environments, such as the deep ocean. Therefore, it is important to investigate underwater microrobot systems consisting of a mother submarine and microrobots to enable long-distance operation of underwater microrobots (Ostergaard et al., 2001; Kim et al., 2004).

As shown in Figure 5, we use an unmanned undersea vehicle (UUV) as the mother submarine in the microrobot system. The mother submarine should have enough space to carry several microrobots. When they receive control signals, the microrobots can be released from the body of the mother submarine. The microrobots should move to the target area while maintaining a certain distance from one another. The mother submarine should have a simple structure and small size, and should be driven by micro motors (Lin and Guo, 2010).

3 Development of a fish-like microrobot

The low actuating voltage and quick bending responses of ICPF are considered very attractive for the construction of various types of actuators and sensors. Because a microrobot with an ICPF actuator uses a small battery, the microrobot can be put into the body of a multi-microrobot system. And we designed a centimetre-scale fish-like microrobot driven by ICPF actuators, shown in Figure 6. This robot has one ICPF actuator, a fin, and a power-supply switch. The ICPF actuator swing and the microrobot can do forward motion because of the small resistance of water.

Figure 7 shows the hardware components of the biomimetic fish-like microrobot. It consists of a waterproof, Omron relay-control system, a lead connector, the ICPF actuator, a power supply for the AVR system and ICPF actuator, the AVR min-system, AVR microprocessor, infrared receiver, power-supply switch, and batteries for the AVR and ICPF actuators.

We used the AVR ATmega16 as the microrobot control unit, and Omron relay switches are used to change the input voltage at the ICPF actuator. The control signal of the ICPF actuator was a square-wave signal, which could efficiently drive the microrobot. The AVR control system and actuators are voltage supplied. The infrared ray receiver shown in Figure 8 was used to connect the microrobot to the mother submarine or other microrobots. The microrobot was designed to be modular, and connector leads were used so that we could easily replace one section of the microrobot. The power supply switch was located on the outside of the microrobot (Gao and Guo, 2010).

Figure 6 Exterior view of the fish-like microrobot (see online version for colours)

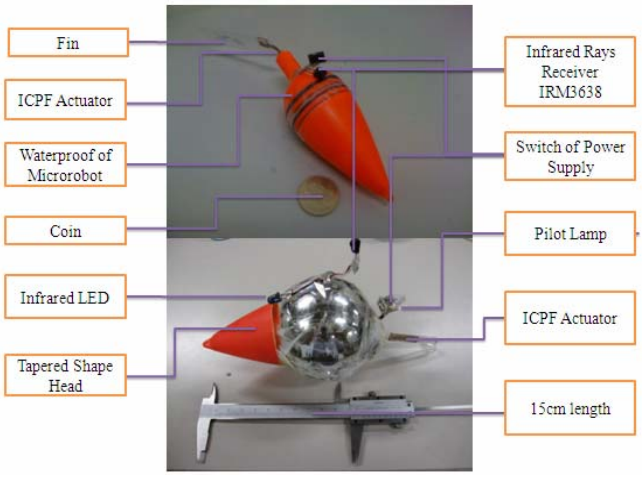

Figure 7 AVR system and Omron relay-control circuit (see online version for colours)

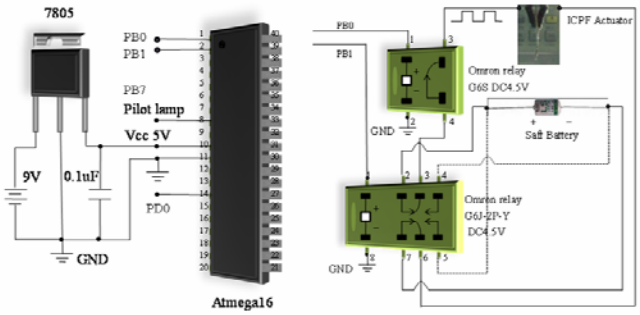

Figure 8 Infrared receiver IRM3638 and L-53F3BT infrared LED launching circuit (see online version for colours)

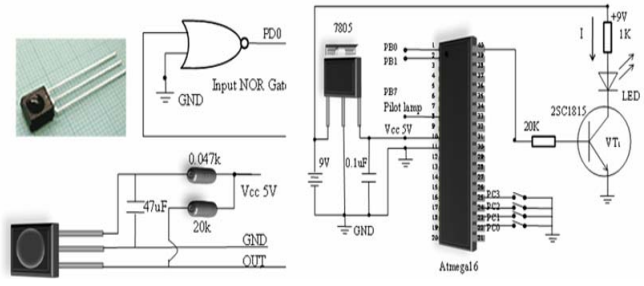

Note: The carrier frequency of the IRM3638 system was 38 KHz, and the peak wavelength was 940 nm, with a pulse width of 400 to 800 us.

A 38-KHz communication protocol was used to facilitate communication between robots and the mother submarine as well as to detect underwater obstacles. When no signal was received, the output of the IRM3638 was high voltage, and it became low voltage when received infrared signals.

Figure 9 shows the buoyancy device, SMA actuator is used to control the device. When water is push out of the body, the microrobot floats up. Also, we can add a certain control voltage to keep the balance of the microrobot.

Figure 9 Buoyancy device of the microrobot (a) shows the battery, SMA actuators and tank of the buoyancy device (b) is the top view of the buoyancy device (see online version for colours)

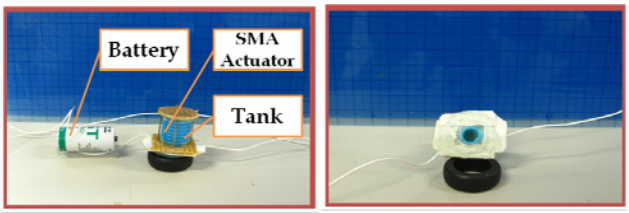

(a) (b)

4 Analysis of the infrared control signal

The Omron relay system used to provide the square-wave drive signal has a delay of 5 to 10 ms, and this must be taken into account to describe the motion of the actuator. Because there are four relays, it is possible for them to all be on at once, providing short-circuit current path, which would damage the battery. This can be avoided by limiting the on and off times for the drive signals.

The open-loop control signal to the ICPF is usually instabilities, so we must wait for the ICPF actuator to swing back into the neutral position and add a new control signal.

The infrared control signal is a square-wave, as shown in Figure 10. When the duty cycle is 0.5 and the period is 1.2 ms, each period should contain at least ten pulses of the 38 KHz infrared signal. The signal is high for 600 µs; one period at 38 kHz lasts for 26.3 µs, resulting in a single square output pulse from the IRM3638. This defines a logical '1' within the communications protocol; similarly, a 600 µs long low signal defines a logical '0'. As an example, the binary number '0B11000011' is shown encoded in Figure 11. The infrared communication code is in five parts, consisting of the start code, address code, address-reverse code, data code, and data-reverse code.

Figure 10 The 38-KHz infrared ray transmitted data and definition of logical '1' and logical '0' (see online version for colours)

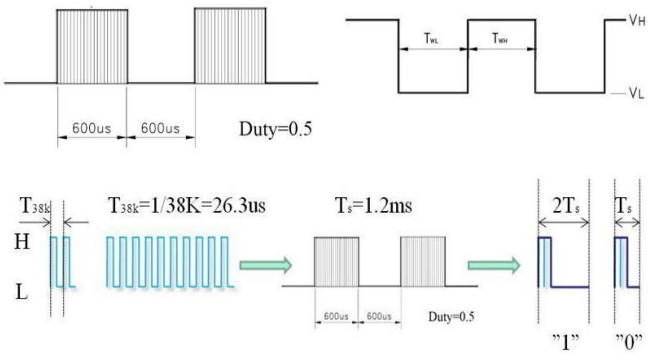

Figure 11 The infrared ray control code and ICPF actuator control signal corresponding to the actuator swing at 0.5 Hz (see online version for colours)

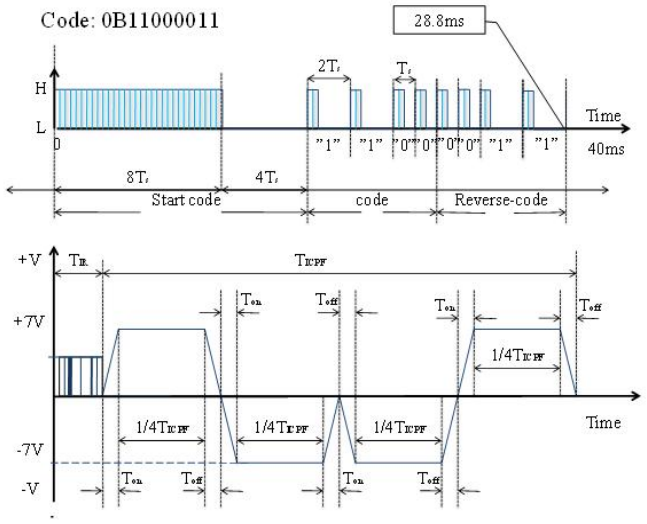

Figure 11 shows the infrared ray control code and control signal corresponding to an ICPF actuator swing at 0.5 Hz. Figure 12 shows the infrared ray control code and control signal corresponding to a quick swing of ICPF actuator. Figure 13 shows the infrared ray control code and control signal corresponding to an ICPF actuator swing to the left. Figure 14 shows the infrared ray control code and control signal corresponding to an ICPF actuator swing to the right.

Figure 12 The infrared ray code and ICPF actuator control signal corresponding to a quick swing of the actuator (see online version for colours)

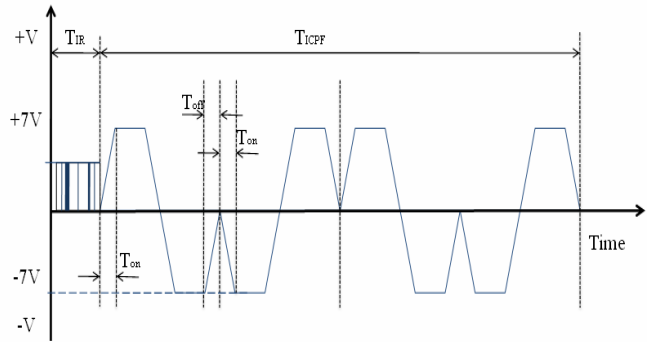

Figure 13 The infrared ray code and ICPF actuator control signal corresponding to the actuator swing to the left (see online version for colours)

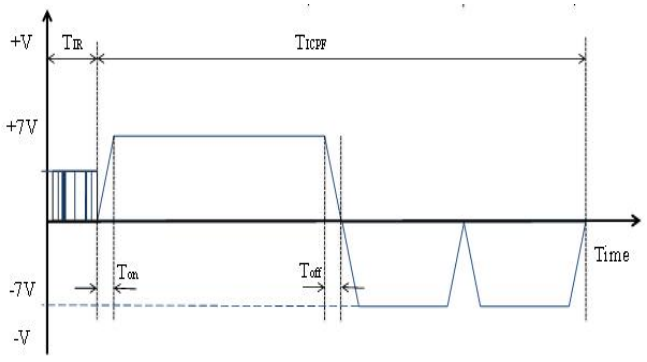

Figure 14 The infrared ray code and ICPF actuator control signal corresponding to the actuator swing to the right (see online version for colours)

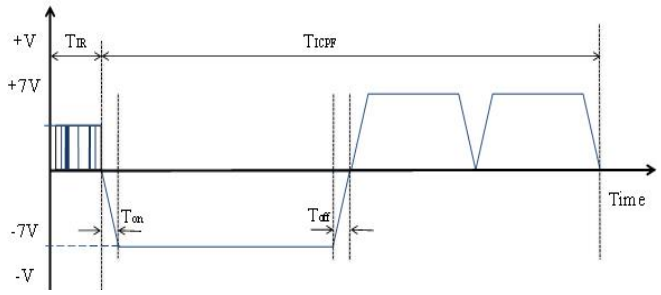

T_{IR} is the time taken to receive the infrared code, and T_{ICPF} is the time for an entire period of ICPF actuator control signals. Here, we have considered the on/off time of the Omron relay. It takes 40 ms to receive the infrared control signal. As shown in Table 1, we defined the binary notation corresponding to the different underwater microrobots: Bit7 and Bit6 represent the name of the microrobot, Bit5 and Bit4 is the motion instruction and Bit3–Bit0 are the reverse codes to correct the binary code.

Table 1 Binary code table

The binary notation code of underwater microrobots					
Bit7, Bit6	*Bit5, Bit4*				*Bit3–Bit0*
Robots	*(A)*	*(B)*	*(C)*	*(D)*	*Reverse code*
00	00	01	10	11	11XX
01	00	01	10	11	10XX
10	00	01	10	11	01XX
11	00	01	10	11	00XX

Table 2 Motion control of the microrobot

Stop	No infrared control signal is received
Motion (A)	Normal forward movement
Motion (B)	Turning to the left
Motion (C)	Turning to the right
Motion (D)	Fast forward movement

5 Path-planning and optimisation

We proposed a primary spiral particle pathway searching approach to search for particles in the pathway. This searching approach is similar to the free-space method and the grid method.

As shown in Figure 15, we need to establish a 3-D space coordinate system to locate the positions of the start point, the obstacle, and the target point. We established the rectangular coordinate system of 3-D space at the start point O (0, 0, 0), then defined the target point T (0, 0, z_t) at the Z axis; and defined O_1, O_2,…, O_p as obstacle sphere centre.

The general spiral curve equation can be represented by polar coordinates as follows:

$$\begin{cases} \theta(t) = a \cdot t^{\lambda} \\ l(t) = ab \cdot t^{\lambda} \end{cases} \tag{2}$$

where a, b, λ are parameters determine the shape of spiral curve, t is the variable parameter, and $\theta(t)$ and $l(t)$ are the polar coordinates of particles.

Figure 15 The rectangular coordinate system

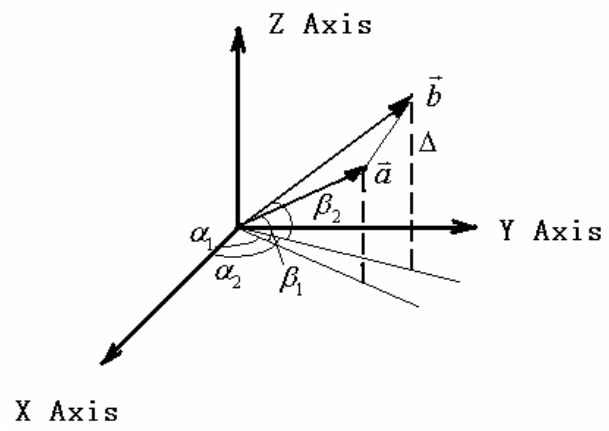

Figure 16 shows spiral curves with different parameters. We can choose different curves to help search potential particles, and the coordinates of points on the spiral curve can be calculated using equation (3).

$$\begin{cases} x_{ij} = l(t) \cdot \cos(\theta(t)) \\ y_{ij} = l(t) \cdot \sin(\theta(t)) \end{cases} \tag{3}$$

Figure 16 Spiral curves with different parameters (a) a = 10, b = 0.16, λ = 0.45 (b) a = 10, b = 0.16, λ = 0.65 (c) a = 10, b = 0.16, λ = 0.85 (d) a = 10, b = 0.36, λ = 0.65 (see online version for colours)

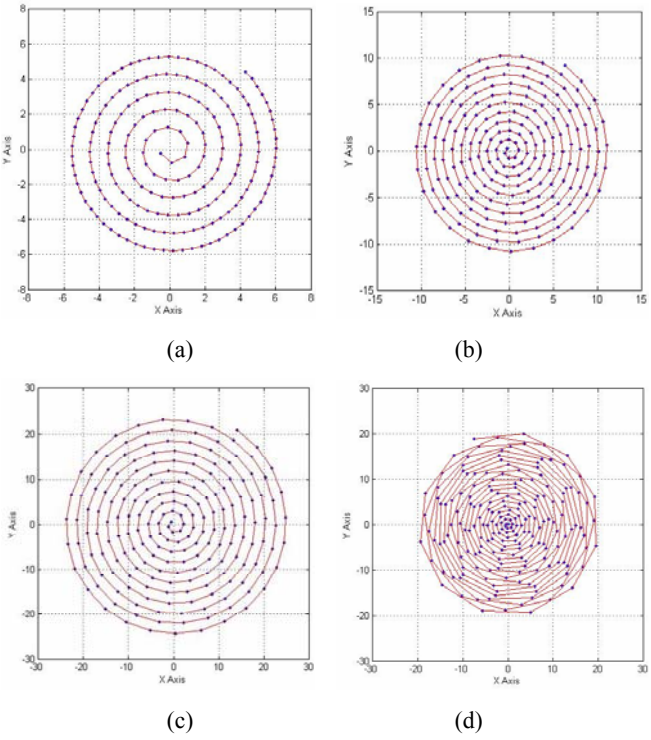

(a) (b)

(c) (d)

In the case of circles cut by sphere obstacles, in the area of circles particles are not in the pathway, so we have to delete them according to the distance between the centre O_k and the particle P_i (Guo and Gao, 2009):

$$|O_k P_i| > r_{Ok} \tag{4}$$

Then other particles lie in the efficient pathway:

$$|O_k P_i| < r_{Ok} \tag{5}$$

Numerous particles are possible in the shortest pathway found by the spiral particle pathway searching approach. We can easily find the coordinates of each particle using equation (6).

$$\begin{cases} x_{ij} = ab \cdot t^{\lambda} \cdot \cos\left(a \cdot t^{\lambda}\right) \\ y_{ij} = ab \cdot t^{\lambda} \cdot \sin\left(a \cdot t^{\lambda}\right) \\ z_{ij} = z_{pj} \end{cases} \tag{6}$$

When we chose parameters: $a = 10$, $b = 0.16$, $\lambda = 0.65$, we can obtain the coordinates of particles:

$$\begin{cases} x_{ij} = 0.36 \cdot i^{0.65} \cdot \cos\left(2.24 \cdot i^{0.65}\right) \\ y_{ij} = 0.36 \cdot i^{0.65} \cdot \sin\left(2.24 \cdot i^{0.65}\right) \\ z_{ij} = 0.5 \cdot j \end{cases} \tag{7}$$

$$i = 1, 2, 3 \cdots m \qquad j = 1, 2, 3 \cdots n_p$$

Sometimes, we want to get best results but cost less. And shortest path-planning and optimisation is significant. Now we can use PSO algorithm to optimise the result (Kennedy, 2002).

Figure 17 shows particles movement trends to the global best position. The particle numbers is 30, and the object function $F(t)$ of the PSO algorithm is as follows:

$$\begin{aligned} F(t) &= f\left(x_j(t)\right) \\ &= \sum_{j=2}^{n_p} \sqrt{\left(x_j(t) - x_{j-1}(t)\right)^2 + \left(y_j(t) - y_{j-1}(t)\right)^2 + \left(z_j - z_{j-1}\right)^2} \end{aligned} \tag{8}$$

$$\begin{cases} x_j(t) = x_{ij} + \Delta x_j(t) \\ y_j(t) = y_{ij} + \Delta y_j(t) \\ z_j(t) = z_{ij}(t) \end{cases} \quad \begin{cases} i = 1, 2, 3 \cdots m \\ j = 1, 2, 3 \cdots n_p \end{cases} \tag{9}$$

$$\begin{cases} \Delta x_{ij}(t) = \mu_1 \cdot t^{0.65} \cdot \cos\left(\mu_2 \cdot t^{0.65}\right) \\ \Delta y_{ij}(t) = \mu_1 \cdot t^{0.65} \cdot \sin\left(\mu_2 \cdot t^{0.65}\right) \end{cases} \tag{10}$$

where μ_1 and μ_2 are contents, the spiral curve is small enough to ensure the position of particle $P_j(i)$ optimised.

When we use PSO algorithm to optimise the pathway, we have to choose different parameters, such as inertia weight w, $c1$, and $c2$ and so on, those parameters can influent the results of the optimisations. As shown in Figures 18 and 19, the function optimised from 40 to 36, and at last we choose the parameters w equal to 0.7298 and N equal to 40. Also, for some reason, the PSO algorithm is not the fastest one to optimise the pathway, so that we could use some else faster PSO algorithm (Suganthan, 1999; Eberhart and Shi, 2001).

Figure 17 Trends in particle movement to the global best (see online version for colours)

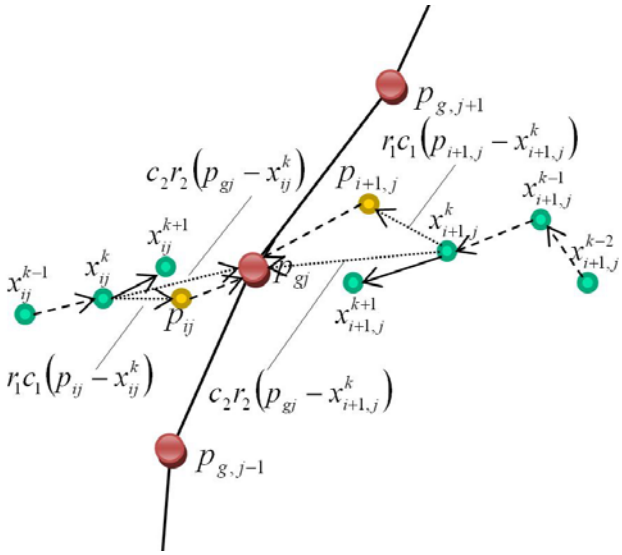

Figure 18 Function results with different inertia weight w (see online version for colours)

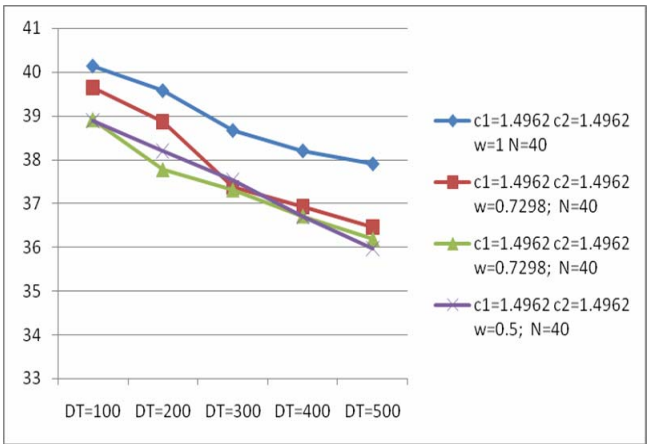

Figure 19 Function results with different generation N (see online version for colours)

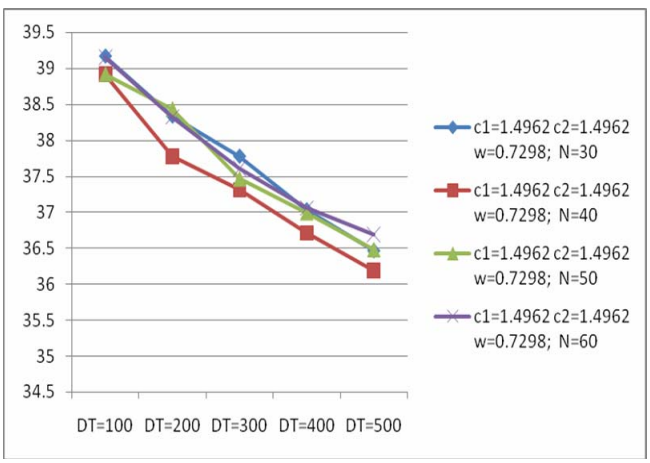

The primary spiral particle pathway searching approach to search for particles in the pathway in the plane of parallel subspace. We used the object function of the PSO algorithm and use MATLAB to calculate the particles in order to search for the best path to the target point in three-dimensional space. We determined the shortest pathway for a single robot, optimised by PSO. The path-planning and optimisation simulation results of an underwater microrobot in 3-D space are both possible and efficient.

We simulated the movement of group of microrobots, and optimise the path-planning results using PSO algorithm. Figure 20 shows OpenGL simulation results of microrobots do the rotational movement. Each microrobot should adjust the velocity to keep them together in a triangle formation in 3-D space.

Figure 20 OpenGL simulation results about several microrobots doing the rotational movement (a) robot A, B, C and D are in a group (b) shows us robot (B), (C) and (D) are following the robot (A) and doing the rotational movement in a triangle formation all the time (see online version for colours)

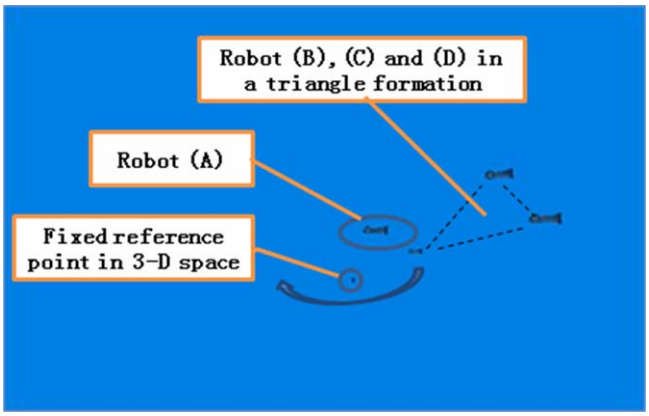

(a)

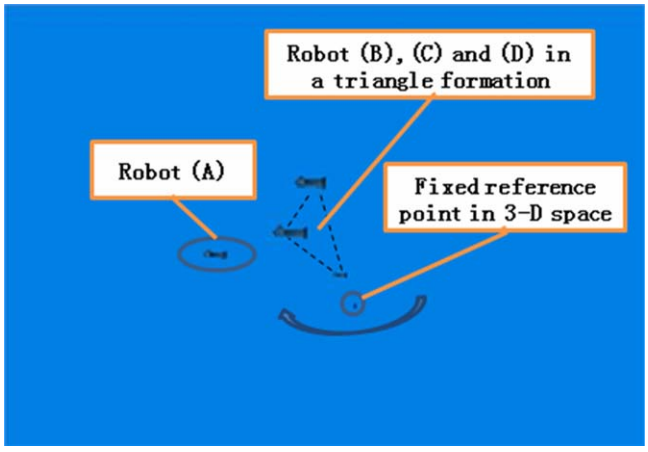

(b)

6 Experimental results

Figure 21 illustrates flow-chart used in the AVR microprocessor to control the microrobot. First, we include header files and define time-delay, key-scanning, and motion functions. In the main function, we initialise ports A and B, define them as input or output ports, and then illuminate the pilot lamp to show that the AVR is functioning. We then enter a loop, in which we return the value of key-scanning function, and if it is false, continue to check until the value becomes true. If the start code is found, we begin to record the code eight times, wait for 500 μs each time. The signal is cross-referenced against the pre-defined signal codes to determine which motion function should be carried out, and the ICPF actuator is driven accordingly. Finally, the actuator is returned to its initialisation state and powered off.

Figure 21 Flow chart illustrating the embedded program in the AVR microprocessor used to control the microrobot (see online version for colours)

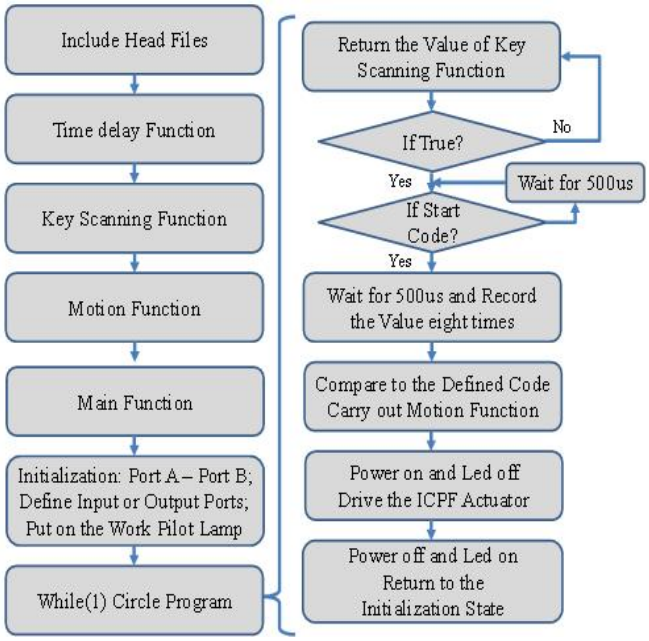

The average speed achieved by the microrobot is shown in Figure 22. In each case, four different configurations of the microrobot body were investigated, and we found that the maximum velocity was achieved using a 25 × 5 mm tapered body, with a 0.4 mm ICPF actuator.

Figure 22 Average speed of the underwater microrobot (using a 0.4 mm ICPF actuator) (see online version for colours)

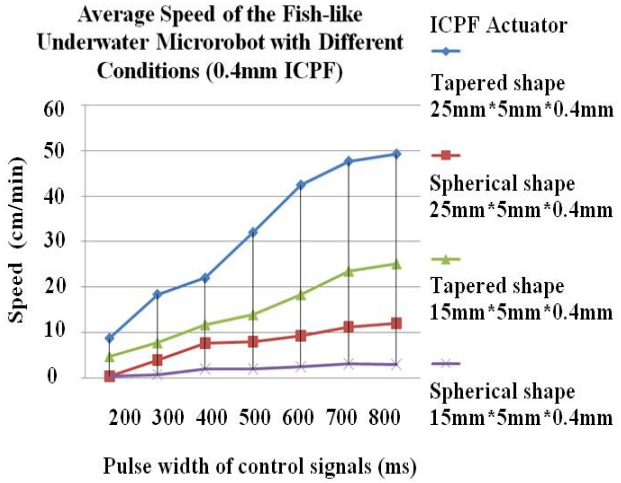

Figure 23 The rotational movement of the underwater microrobot (a) a microrobot is doing rotational movement; t = 0 s [(b) and (c)] shows the process of the microrobot turn the right direction by the swing of ICPF actuator (b) t = 10 s (c) t = 20 s (see online version for colours)

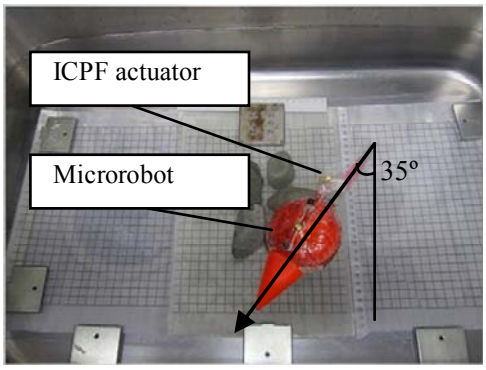

(a)

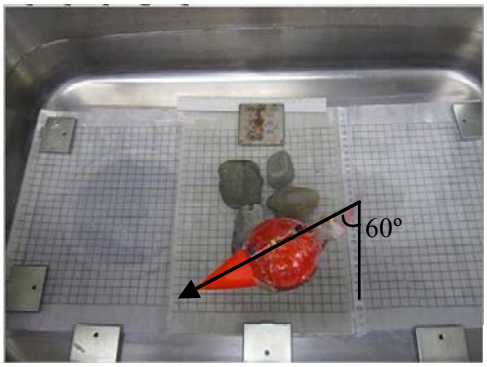

(b)

Figure 23 The rotational movement of the underwater microrobot (a) a microrobot is doing rotational movement; t = 0 s [(b) and (c)] shows the process of the microrobot turn the right direction by the swing of ICPF actuator (b) t = 10 s (c) t = 20 s (continued) (see online version for colours)

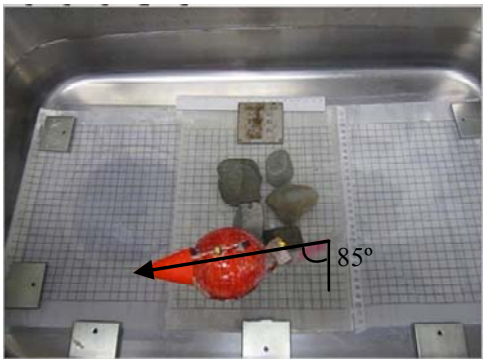

(c)

We used video recording to monitor the trajectory of the microrobot. Figure 23 shows the underwater microrobot moving forward and then changing the direction to the right, the velocity of the microrobot reached 2 cm/s. Although the AVR system used an open-loop control method and no detect feedback information from the ICPF actuator, however, the additional control features allowed the ICPF actuator operation to be stable. Figure 24 shows us the microrobot to float up and down. Figure 25 demonstrates the use of communication system to control several microrobots travelling in formation in a straight line. We can find those microrobot can be well controlled even using the open-loop control system.

Figure 24 The movement of the underwater microrobot floating up and down by controlling the buoyancy device (a) the microrobot is start to float up; t = 0 s (b) the microrobot float up 10 cm; t = 5 s [(c) and (d)] the microrobot float down to the original start point (b) t = 5 s (c) t = 5 s (d) t = 10 s (see online version for colours)

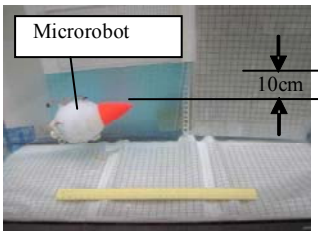

(a)

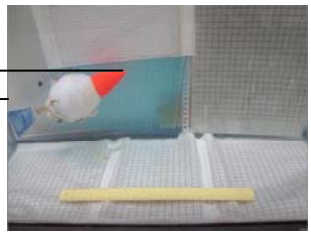

(b)

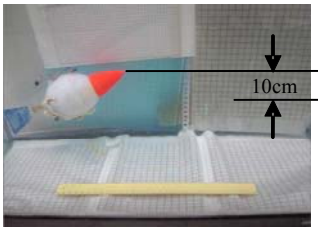

(c)

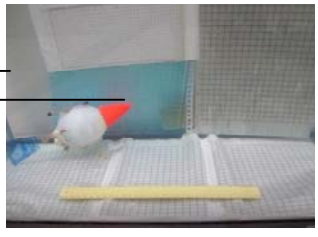

(d)

Figure 25 The movement of three underwater microrobots keep a straight line formation controlled by the infrared communication system (a) those microrobots receive the infrared ray signal and start to move; t = 0 s [(b) and (c)] those three microrobots swim close to the target area and still keep the straight line formation (b) t = 20 s; (c) t = 40 s (see online version for colours)

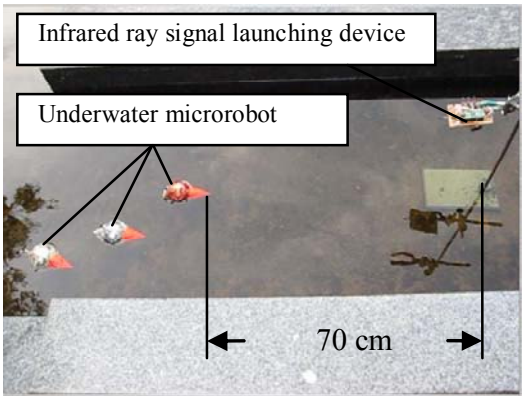

(a)

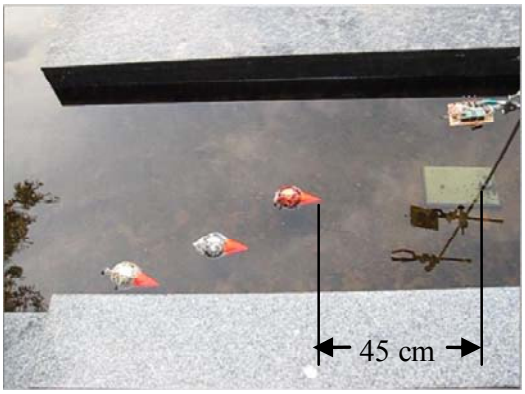

(b)

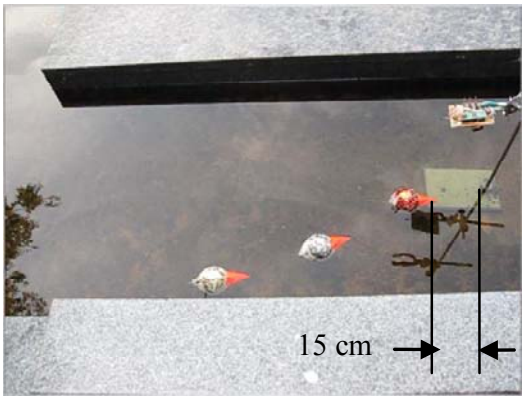

(c)

7 Conclusions and future work

ICPF actuators are low-power devices and so are suitable for microrobot applications because of the favourable battery power requirements. In this paper, we developed the application of ICPF and SMA actuators in underwater microrobot and designed the fish-like microrobot which is consist of ICPF actuator, AVR control system and infrared ray remote control system. Biomimetic fish-like underwater microrobots can be remotely controlled by a larger mother submarine. Each microrobot consists of an AVR minimum-control unit, an infrared communication system, and ICPF actuators. The infrared ray device in the mother submarine communicates with the AVR control system to control the movement of the individual fish-like microrobot.

We also demonstrated wireless control over the trajectory of individual microrobot and dealt with the formation problem in multi-robot systems, analysed the velocity control of three microrobots in a group to keep in a triangle formation. We proposed the primary spiral particle pathway searching approach to search for particles and use PSO to optimise those results. Furthermore, OpenGL simulation results show that path planning using particle swarm optimisation can be applied to automatically navigate underwater obstacles, which will make the system more robust as microrobots find the best path to a given destination. Future work will focus on developing the motion control to realise this multi-robot operation.

Acknowledgements

This research was supported by Kagawa University Characteristic Prior Research Fund 2010.

References

Du, Q., Emelianenko, M. and Ju, L. (2006) 'Convergence of the Lloyd algorithm for computing centroidal Voronoi tessellations', *SIAM Journal on Numerical Analysis*, Vol. 44, pp.102–119

Eberhart, R. and Shi, Y. (2001) 'Particle swarm optimization: developments, applications and resources', *Proc. IEEE Int. Conf. on Evolutionary Computation*, pp.81–86.

Fukuda, T., Kawamoto, A. and Arai, F. (1995) 'Steering mechanism of underwater micro mobile robot', *Proceedings of the 1995 IEEE International Conference on Robotics and Automation*, Vol. 1, pp.363–368.

Fukuda, T., Kawamoto, A., Arai, F. and Matsuura, H. (1994) 'Mechanism and swimming experiment of micro mobile robot in water', *Proceedings of the 1994 IEEE International Conference on Robotics and Automation*, Vol. 1, pp.814–819.

Gao, B. and Guo, S. (2010) 'An infrared ray controlled fish-like underwater microrobot', *INFORMATION: An International Interdisciplinary Journal*, Vol. 13, No. 6, pp.1973–1983.

Gerkey, B. and Mataric, M. (2002) 'Pusher-watcher: an approach to fault-tolerant tightly-coupled robot coordination', *Proceedings IEEE International Conference on Robotics and Automation*, pp.464–469.

Gerkey, B. and Mataric, M. (2002) 'Sold: auction methods for multirobot coordination', *IEEE Transactions on Robotics and Automation*, Vol. 18, No. 5, pp.758–768.

Guo, J. Xiao, N., Guo, S. and Tamiya, T. (2010) 'Development of a force information monitoring method for a novel catheter operating system', *INFORMATION: An International Interdisciplinary Journal*, Vol. 13, No. 6, pp.1999–2009.

Guo, S. and Asaka, K. (2003) 'A new type of micropump driven by a low electric voltage', *International Journal of Acta Mechanica Sinica*, Vol. 20, No. 2, pp.146–1151.

Guo, S. and Wang, J. (2003a) 'Development of a micro intelligent autonomous moving robot', *INFORMATION: An International Interdisciplinary Journal*, Vol. 6, No. 5, pp.583–592.

Guo, S. and Gao, B. (2009) 'Path-planning optimization of underwater microrobots in 3-D space by PSO approach', *Proceedings of the 2009 IEEE International Conference on Robotics and Biomimetics*, pp.1615–1620.

Guo, S., Fukuda, T. and Asaka, K. (2003) 'A new type of fish-like underwater microrobot', *Proc. IEEE/ASME Transactions on Mechatronics*, Vol. 8, No. 1, pp.738–743.

Guo, S., Okuda, Y., Zhang, W., Ye, X. and Asaka, K. (2006) 'The development of a hybrid type of underwater micro biped robot', *Applied Bionics and Biomechanics*, Woodhead Publishing Limited, Cambridge UK, Vol. 3, No. 3, pp.143–150.

Jennings, J., Whelan, G. and Evans, W. (1997) 'Cooperative search and rescue with a team of mobile robots', in *Proc. IEEE Int. Conf. Advanced Robotics*, pp.193–200.

Kamamichi, N., Kaneda, Y., Yamakita, M., Asaka, K. and Luo, Z.W. (2003) 'Biped walking of passive dynamic walker with IPMC linear actuator', *SICE Annual Conference in Fukui*, pp.212–217.

Kennedy, J. (2002) 'Stereotyping: improving particle swarm performance with cluster analyses', *Proc. IEEE Int. Conf. on Evolutionary Computation*, pp.1507–1512.

Kim, S., Clark, J.E. and Cutkosky, M.R. (2004) 'Isprawl: autonomy, and the effects of power transmission', in *Proceedings of CLAWAR*, *Madrid*, *Spain*, pp.22–24.

Klaassen, B., Linnemann, R., Spenneberg, D. and Kirchner, F. (2002) 'Biomimetic walking robot scorpion: control and modeling', in *Proceedings of the ASME Design Engineering Technical Conference*, Vol. 5, pp.1105–1112.

Lelli, F., Frizziero, E., Gulmini, M., Maron, G., Orlando, S., Petrucci, A. and Squizzato, S. (2007) 'The many faces of the integration of instruments and the grid', *International Journal of Web and Grid Services 2007*, Vol. 3, No. 3, pp.239–266.

Lin, X. and Guo, S. (2010) 'Development and evaluation of a vectored water-jet-based spherical underwater vehicle', *INFORMATION: An International Interdisciplinary Journal*, Vol. 13, No. 6, pp.1985–1998.

Mojarrad, M. and Shahinpoor, M. (1997) 'Biomimetic robotic propulsion using polymeric artificial muscles', *Proceedings of the 1997 IEEE International Conference on Robotics and Automation*, Albuquerque, New Mexico, pp.2152–2157.

Nguyen, Q.S., Heo, S., Park, H.C., Goo, N.S., Kang, T., Yoon, K.J. and Lee, S.S. (2009) 'A fish robot driven by piezoceramic actuators and a miniaturized power supply'. *International Journal of Control*, *Automation and Systems*, pp.267–272.

Okuzaki, H. and Osada, Y. (1994) 'Effects of hydrophobic interaction on the cooperative binding of surfactant to a polymer network', *Macromolecules*, Vol. 27, pp.502–506.

Ostergaard, E., Mataric, M. and Sukhatme, G. (2001) 'Distributed multi-robot task allocation for emergency handling', in *Proceedings of IEEE/RSJ International Conference on Robots and Systems*, pp.821–826.

Pan, Q., Guo, S. and Khamesee, M.B. (2008) 'Development of a novel type of microrobot for biomedical application', *Microsystem Technologies*, Springer Berlin Heidelberg, Vol. 14, No. 3, pp.307–314.

Rus, D., Donald, B. and Jennings, J.S. (1995) 'Moving furniture with teams of autonomous robots', in *Proceedings IEEE/RSJ International Conference on Intelligent Robots and Systems (IROS)*, pp.235–242.

Sadeghipour, K., Salomon, R. and Neogi, S. (1992) 'Development of a novel electrochemically active membrane and smart material based vibration sensor/damper', *Smart Materials and Structures*, Vol. 1, pp.172–179.

Shahinpoor, M. (1996) 'Ionic polymeric gels as artificial muscles for robotic and medical applications', *International Journal of Science and Technology*, Vol. 20, No. 1, Transaction B, pp.89–136.

Shahinpoor, M., Bar-Cohen, Y., Simpson, J.O. and Smith, J. (1998) 'Ionic polymer-metal composites (IPMC) as biomimetic sensors, actuators and artificial muscles – a review', *Smart Materials and Structures*, Vol. 7, No. 6, pp.R15–R30.

Shi, L., Guo, S. and Asaka, K. (2010) 'A novel multifunctional underwater microrobot', *Proceedings of the 2010 IEEE International Conference on Robotics and Biomimetics*, pp.873–878.

Stone, P. and Veloso, M. (1999) 'Task decomposition, dynamic role assignment, and low-bandwidth communication for real-time strategic teamwork', *Artificial Intelligence*, Vol. 110, No. 2, pp.241–273.

Suganthan, P.N. (1999) 'Particle swarm optimizer with neighborhood operator', *Proc Congress on Evolutionary Computation*, pp.1958–1962.

Waldner, J-B. (2008) *Nanocomputers and Swarm Intelligence*, ISTE John Wiley & Sons, London, p.205, ISBN 1848210094.

Wei, W. and Guo, S. (2010) 'A PDMS diaphragm micropump using electroosmotic actuation', *INFORMATION: An International Interdisciplinary Journal*, Vol. 13, No. 6, pp.2069–2080.

Ye, X., Gao, B., Guo, S. and Wang, L. (2006) 'Development of ICPF actuated underwater microrobots', *International Journal of Automation and Computing*, Vol. 3, No. 4, pp.382–391.

Ye, X., Zhu, L. and Guo, S. (2010) 'Deformation model of soft tissues for real-time surgical simulation', *INFORMATION: An International Interdisciplinary Journal*, Vol. 13, No. 6, pp.2011–2020.

Zhang, W., Guo S., Asaka, K. (2006) 'Development of a novel type of an underwater microrobot with biomimetic locomotion', *Journal of Applied Bionics and Biomechanics*, Vol. 3, No. 3, pp.245–252.

Zhang, W., Guo, S. and Asaka, K. (2006a) 'A new type of hybrid fish-like microrobot', *International Journal of Automation and Computing*, Vol. 3, No. 4, pp.358–365.

Zhao, Z. and Guo S. (2010) 'Design of an acoustic communication system based on FHMA for multiple underwater vehicles', *Wireless Engineering and Technology*, Vol. 1, No. 1, pp.27–35.